NUMERICAL SIMULATION OF THE THERMAL STRATIFICATION IN A HORIZONTAL PIPE

Moysés A. Navarro, navarro@cdtn.br
Hugo Cesar Rezende, hcr@cdtn.br
Brazilian Nuclear Energy Commission (CNEN/CDTN), Belo Horizonte, 30123-979, Brazil

André A. C. dos Santos, acampagnole@yahoo.com.br
Hermes Carvalho, hermesc2000@yahoo.com.br
Federal University of Minas Gerais, (UFMG/DEMEC), Belo Horizonte, 31270-901, Brazil

Abstract. *Thermally stratified flows cause thermal loading and fatigue relevant stresses in piping systems. The temperature gradient from top to bottom in a horizontal pipe may result in excessive differential expansion from upper to lower parts of the pipe threatening its integrity. Aiming to a better understanding, the one-phase thermal stratification in nuclear reactor piping, numerical and experimental investigations of the phenomenon are in progress at the Nuclear Technology Development Center CDTN/CNEN. Some simulations of the phenomenon under conditions similar to the steam generator injection nozzle of a Pressurized Water Reactor were carried out with a commercial CFD code CFX-10.0 based on the finite volume approach. An optimized mesh and the RNG k-ε turbulence model were used in the simulation. Experiments in the same conditions were used to validate the numerical methodology. The calculated temperature evolution in the thermocouple positions were compared with the experimental results. Both, experimental and numerical results confirmed the occurrence of thermal stratification and of the striping phenomenon, the oscillation of the hot and cold water interface, in the simulated conditions. Despite the satisfactory agreement between the numerical and experimental results, the study suggests additional numerical simulations using better mesh and time step refinement with a LES (Large Eddy Simulation) methodology and other RANS turbulence models.*

Keywords*: thermal stratification, CFD, PWR reactors, turbulence model, nuclear safety*

1. INTRODUCTION

One phase thermally stratified flow is the condition that occurs in a piping, where two different layers of the same liquid at great temperature difference flow separately, without appreciable mixing due to low flow velocities and density difference. This condition results in a varying temperature distribution in the pipe wall and in an excessive differential expansion of the upper and lower parts of the pipe threatening the integrity of the piping system.

Some safety related piping systems connected to reactor coolant systems in operating nuclear power plants are known to be potentially susceptible to thermally stratified flows. Piping systems of PWR-plants typically related with thermal stratification are pressurizer surge lines, emergency core cooling lines, residual heat removal lines and also some segments of the main piping of the primary and secondary cooling loops, like the hot and cold legs in the primary and the steam generator feedwater piping in the secondary, (Häfner, 1990, Ware and Shah, 1995 and Schuler and Herter, 2004). Temperature differences of about 200 °C can be found in a narrow band around the hot and cold water interface. To assess potential piping damage due to thermal stratification, it is necessary to determine the transient temperature distributions in the pipe wall.

The driving parameter considered to characterize flow under stratified regime due to difference in specific masses is the Froude number, given by:

$$Fr = \frac{U_0}{\left(gD\,\Delta\rho/\rho_o\right)^{1/2}} \tag{1}$$

where,
U_0 is the average velocity of the injection water, in [m/s];
g is the acceleration of the gravity, in [m/s^2];
D is the inner diameter of the tube, in [m];
$\Delta\rho$ is the difference between the densities of the hot and cold water, in [kg/m^3]; and,
ρ_o is the density of the cold water, in [kg/m^3].

The thermal stratification at this nozzle occurs in a Froude number range from ~0.02 to ~0.2 (Poussim and Holcblat, 1995). This paper summarizes an experimental and a numerical methodology developed for the simulation of one phase thermally stratified flow in a nuclear reactor steam generator nozzle. The tests were carried out at different Froude numbers within the appropriate range.

2. EXPERIMENTAL METHODOLOGY

Figure 1 shows a diagram of the experimental facility test section. A vessel simulates the steam generator tank and a stainless steel piping (D = 0.1223 m) with a vertical to horizontal curve, simulates the steam generator injection nozzle. Both the vessel and the piping are filled with hot water and cold water is injected with a low flow rate through a bottom nozzle at the end of the vertical pipe. The water leaves the piping through eleven upper holes at the horizontal segment of pipe inside the vessel.

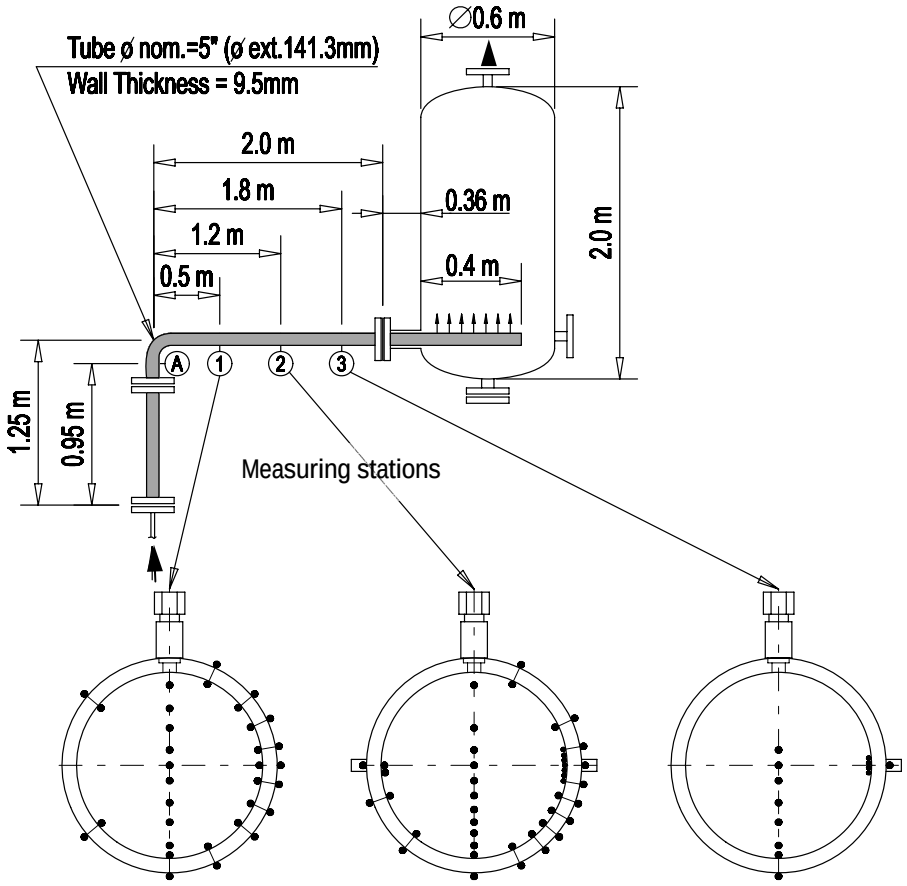

Figure 1. Diagram of the experimental facility test section and thermocouple distribution on its measuring stations 1, 2, 3 and A.

Wall and fluid temperatures are measured with type K thermocouples 0.5 mm in diameter, distributed in three measuring stations (1, 2, 3). In each measuring station fluid thermocouples were positioned along the tube vertical diameter and along the inner wall, 3 mm away from the wall. Wall thermocouples were brazed along the outer wall. The water temperature was also measured with type K thermocouples in the injection piping and in the cold water tank. The injection water flow rate was measured with an orifice plate and a differential pressure transducer. A gauge pressure transducer is used to measure the pressure of the system.

This paper presents results of three tests and comparisons with numerical simulations. Table 1 shows the setting parameters values for the three tests.

Table 1 – Setting parameters for the three tests

Fr	Flow rate [kg/s]	P [bar]	T_{hot} [°C]	T_{cold} [°C]
0.063	0.352	21.1	218.3	39.3
0.146	0.756	21.2	219.2	31.7
0.205	1.06	21.2	219.0	26.5
δ^1	0.03	0.5	2	2

1- Global uncertainty

3. NUMERICAL METHODOLOGY

Two main simplifications in the geometry of the test section, hachured in Fig. 1, were assumed in the simulations: a) the omission of the flanges; b) the omission of the vessel and the assumption of the same boundary condition adopted in the rest of the test section (adiabatic) for the pipe contained in the vessel. The numerical simulation used a commercial CFD code CFX 10.0 (2005) based on the finite volume method. Two simulation domains were created: one solid, corresponding to the pipe, and one fluid for the water in its interior. A vertical symmetry plane along the pipe was adopted to reduce the geometry in one half, reducing the mesh size and minimizing processing time. An unstructured mesh with tetrahedral elements was defined inside the pipe. Two layers of prismatic structured volumes were built close to the surfaces in the solid and fluid domains. Located mesh refinement in the regions of the inlet nozzle and of the outlet holes were necessary due to the local contraction and expansion of fluid that generate high pressure and speed gradients in these regions. Simulations were performed with several refinement levels before adopting a pattern of appropriate mesh. Figure 2 presents details of the mesh adopted for the simulation, with 1,098,451 elements in the fluid domain and 630,389 elements in the solid domain. The initial conditions used for the numerical simulation were the same obtained in the experiment for piping wall temperature, hot and cold water temperature and internal pressure. The three experimental flow rates presented in Tab. 1 were simulated. Water properties like density, viscosity and thermal expansivity were adjusted by regression as function of temperature with data extracted from the Table IAPWS-IF97, in the simulation range (25 ^{o}C to 221 ^{o}C). No heat transfer was considered through the external wall of the pipe (adiabatic wall boundary condition). The RANS - Reynolds Averaging Navier-Stokes equations, the two equations of the RNG k-ε turbulence model, with scalable wall functions, the full buoyancy model and the total energy heat transfer model with the viscous work term were solved. The simulations were performed using parallel simulation on two personal computers Pentium IV HT with 3 Ghz processor, 4 Gb of RAM and 100 Mbps ethernet card. Time step, total transient time and total processing time of each flow rate simulated are presented in Tab. 2.

Table 2 – Simulation characteristics.

Flow rate [kg/s]	Time step [s]	Total transient [s]	Total processing time [h]
0.352	0.06 - 0.12	191	720
0.756	0.05 - 0.1	183	696
1.06	0.08	112	672

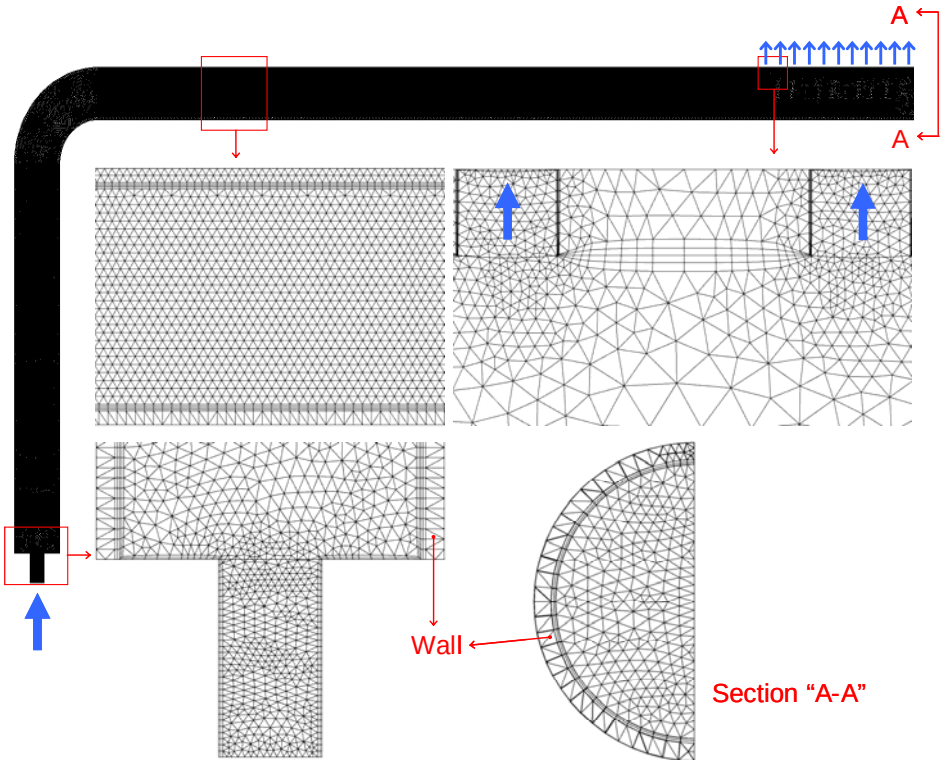

Figure 2. Mesh details.

4. RESULTS

Experimental results were synchronized with the numerical results at the instant when the cold water front reaches the position of thermocouple A. Figure 3 shows the experimental and numerical temperature behaviors in the lowest thermocouple positions of the vertical probes in the measuring stations 1 (T1S08), 2 (T2S08) and 3 (T3S05), respectively, for the three flow rates evaluated. The temperatures fall successively at the probes 1, 2 and 3, due to the arrival of the cold water front at each probe position.

Flow rate 0.354 kg/s:

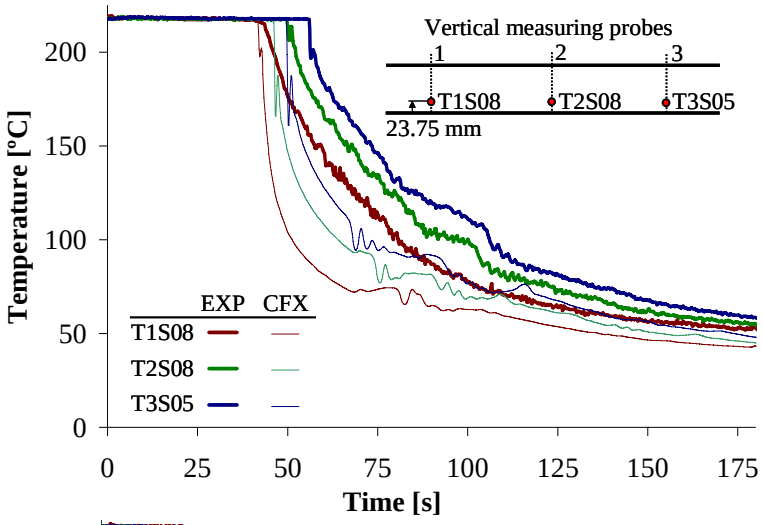

Flow rate 0.756 kg/s:

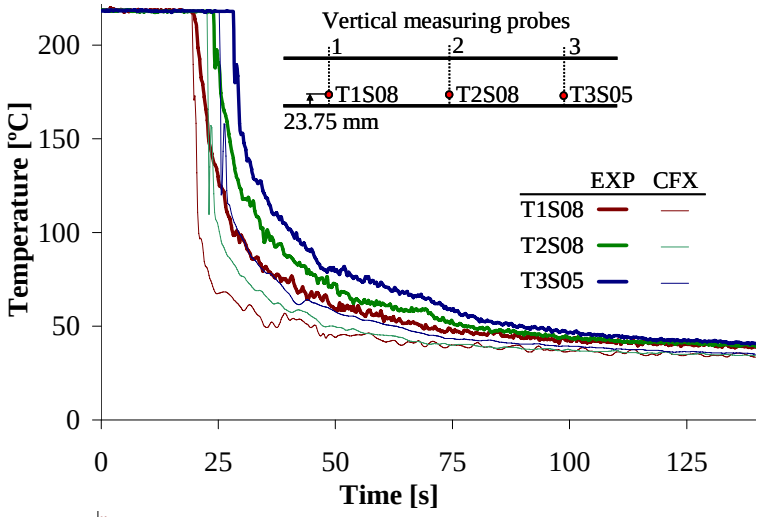

Flow rate 1.06 kg/s:

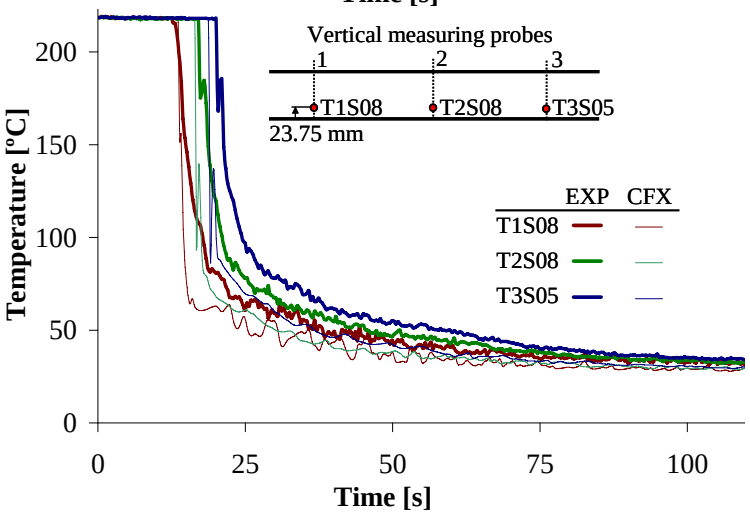

Figure 3. Temperature evolutions along the lower region of the horizontal pipe for three flow rates.

Observing the three figures it is possible to note that the arrivals of the cold water front at the lower thermocouple positions obtained with the numerical simulation occurred earlier than detected experimentally. The difference between both the results increases with the distance from position A. At measuring station 3 the difference varies from 6 s for the lowest flow rate (0.354 kg/s) to 1.5 s for the highest flow rate (1.06 kg/s). The figure shows also that the temperature drop due to the arrival of the cold water front is more abrupt in the numerical results than in the experimental results. This difference decreases as the flow rate increases. Figure 4 shows the temperature evolutions at middle high thermocouple positions at the three measuring stations for the three flow rates.

Flow rate 0.354 kg/s:

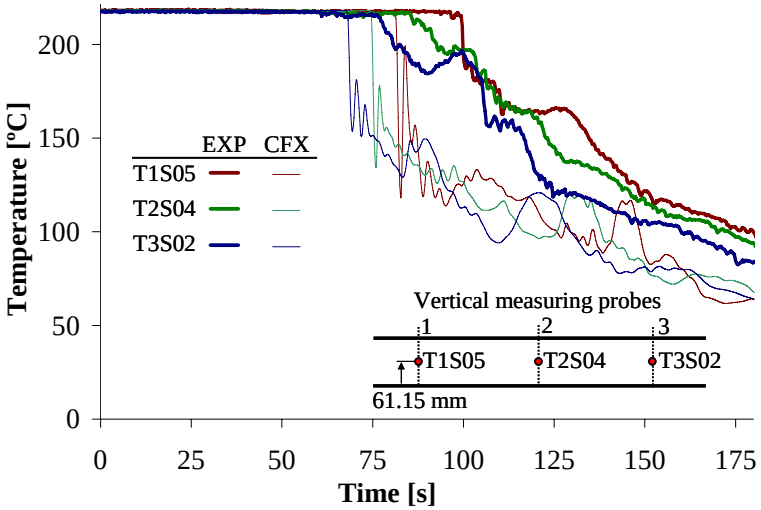

Flow rate 0.756 kg/s:

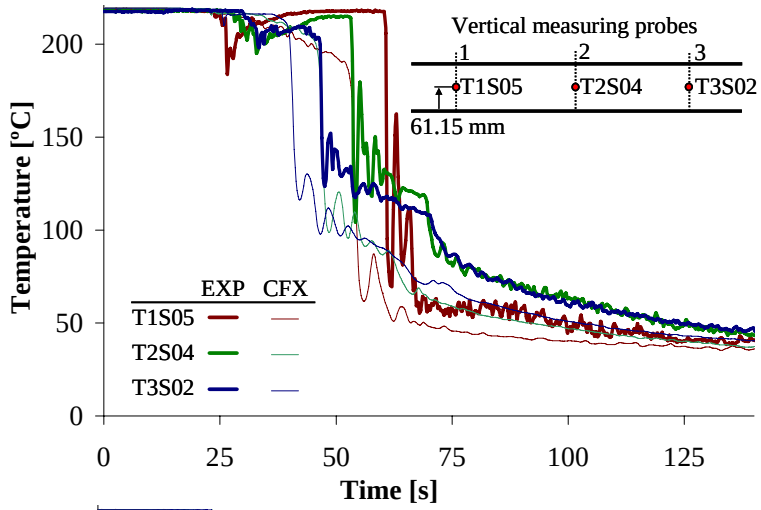

Flow rate 1.06 kg/s:

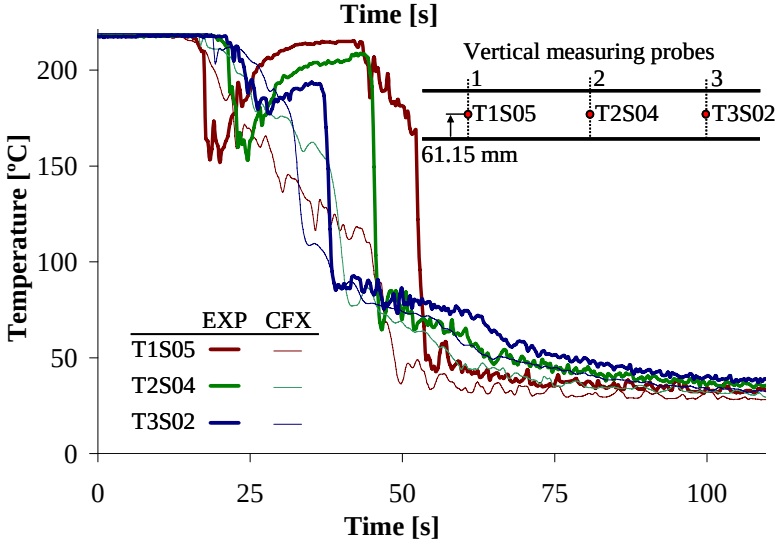

Figure 4. Temperature evolutions along the middle region of the horizontal pipe for three flow rates.

At the flow rate of 0.354 kg/s it can be observed that the thermocouple in measuring station 3 (T3S02) was cooled before the thermocouple in measuring station 2 (T2S04) and the latter before the thermocouple in measuring station 1 (T1S05). At the other flow rates the experimental results show a successive initial cooling in thermocouples T1S05, T2S04 and T3S02 followed by a sudden successive cooling in thermocouples T3S02, T2S04 and T1S05. The first and initial cooling was not observed in the numerical simulation.

The numerical results show that the cold water front hits the wall at the end of the horizontal pipe and a part of the cold water returns through the pipe in the opposite direction as a second cold water front. Figure 5 shows the cold water front evolution for the flow rate of 0.756 kg/s obtained with CFX. A change in the direction of the cold water front after it reaches the end of the tube can be observed.

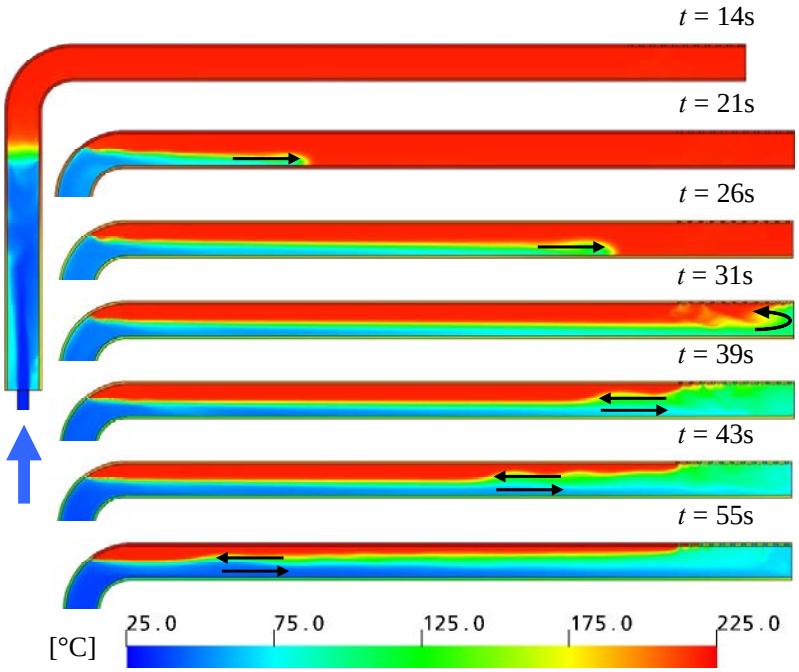

Figure 5. Temperature contours at different times for flow rate 0.756 kg/s.

Figure 6 shows the velocity *u* profiles along the vertical diameter, corresponding to measuring station 2, at different times obtained from the numeric simulation performed with flow rate of 0.756 kg/s. A visualization of the flow behavior with velocity vectors and temperature contours at the same times is also shown in Fig. 6. Initially, at 14 s, the upper velocity profile is almost uniform showing lower velocities at the lower section of the tube. At 23.2 s the arrival of the cold front, with a high velocity, causes the upper hot fluid to shift its flow direction, generating a stratified countercurrent flow that is clearly visualized at 32 s, after the passage of the cold front. This stratified countercurrent flow was also observed in the simulations performed with the other flow rates. When the cold front reaches the end of the horizontal tube, the impact with the wall produces a second cold front that propagates in the opposite direction of the tube. At 47 s the second cold front reaches the vertical measuring probe station 2. Flows in two directions around the cold front in the hot layer can be seen. At 57 s lower velocities of the middle layer on account of the second cold front were observed.

Figure 7 shows the details of the flow behavior and its effects on the temperature at the position of thermocouple T2S04 obtained from both experiments and the numerical simulation at flow rate 0.756 kg/s. The position T2S04, in the middle of the vertical diameter, is marked in the pictures. Figure 7 shows that at 27 s of the experimental simulation, the arrival of the first cold front provokes a brief temperature drop which is not predicted numerically. As seen in Fig. 6, the first cold front at 23.2 s shows a “head”, a small region at the beginning of the front that has a larger height of influence than the rest of the front due to resistance of the flow to mixture. In the experiment a “head” is probably formed causing the fluid temperature to drop at the thermocouple position and to rise again after it has passed. The numerical simulation predicts a smaller “head’ of the cold front and therefore does not predict correctly the brief temperature drop. When the second cold front arrives at the thermocouple position it causes an abrupt drop of temperature shown experimentally at time 53.2 s and numerically at time 46 s. After the arrival of the second front the highly unstable interface between the hot and cold layer causes oscillations of temperature known as thermal striping observed in both experimental and numerical simulations. As can be observed in Fig. 7, from the numerical simulation time of 49 s the thermal striping is predicted as a behaved wave form oscillation. The prediction differs from the experimentally observed oscillations with larger amplitudes. Even so the prediction is reasonably accurate and is able to enlighten many of the experimentally observed phenomena.

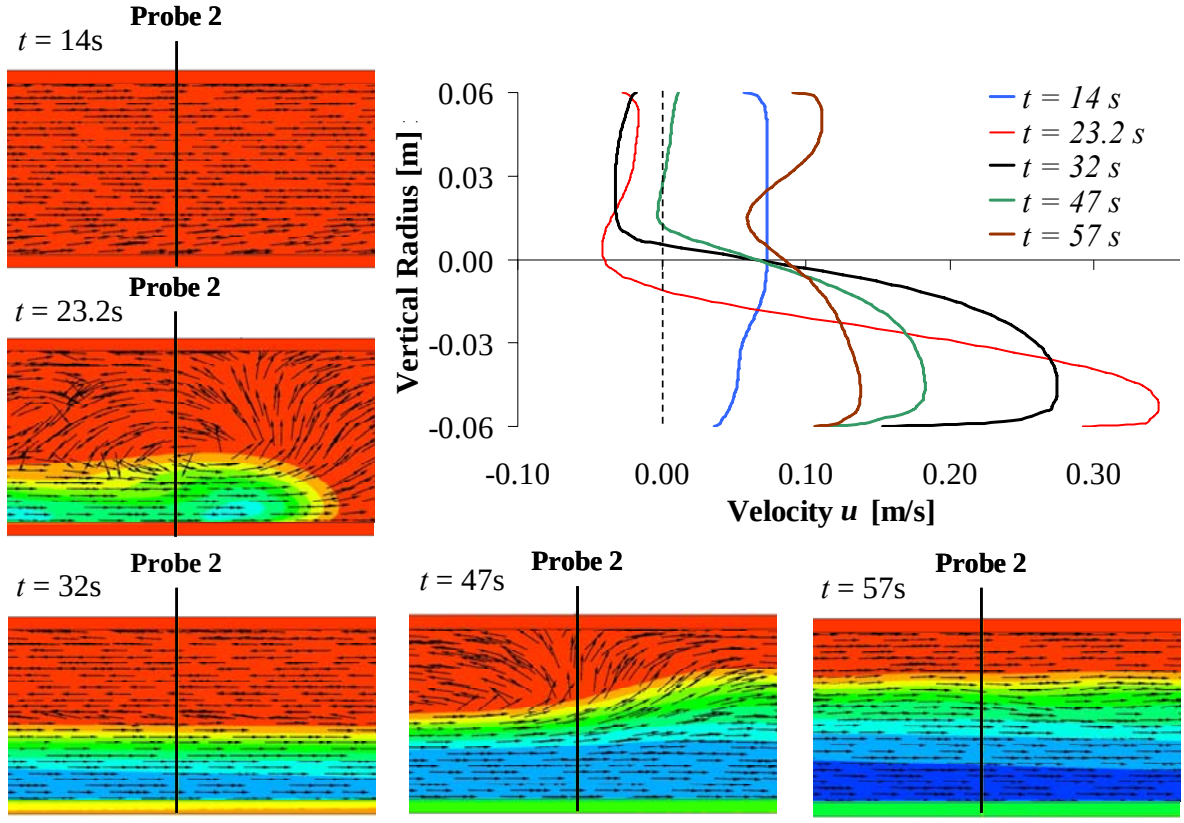

Figure 6. Velocity profiles and vector visualization at different times for flow rate 0.756 kg/s.

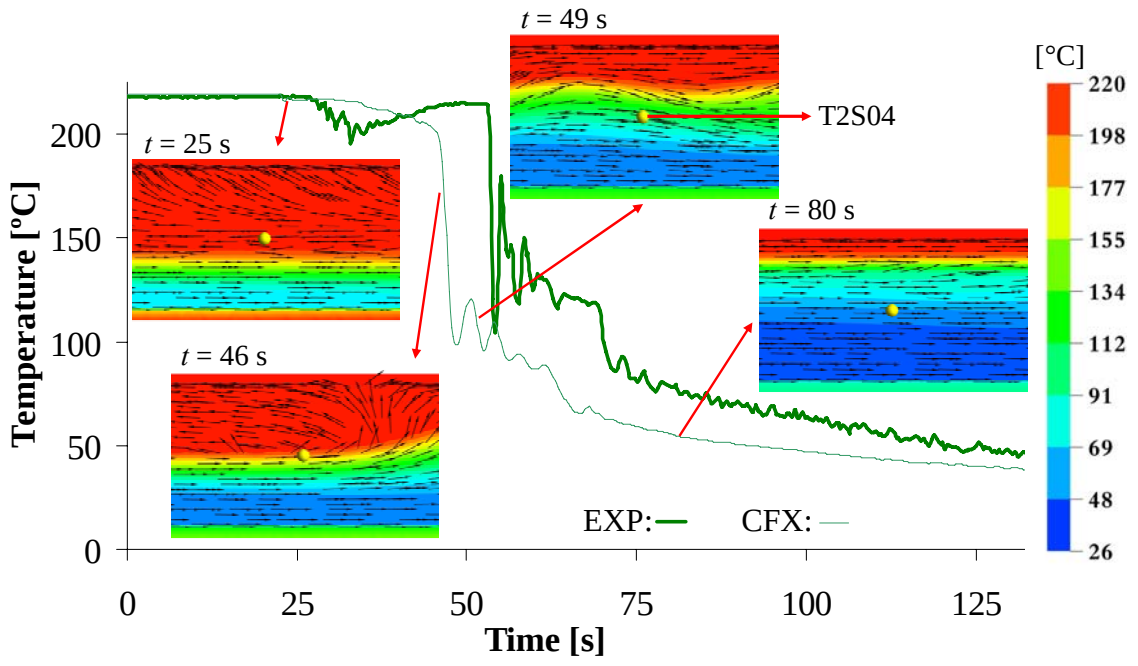

Figure 7. Velocity and temperature profiles at different times for flow rate 0.756 kg/s.

Figures 8 shows the temperature evolutions at higher thermocouple positions at the measuring stations 1 and 2 for the flow rates of 0.354 kg/s and 0.756 kg/s. In both results, the arrivals of the cold water front at thermocouple T2S02 position obtained with the numerical simulation were earlier than detected experimentally.

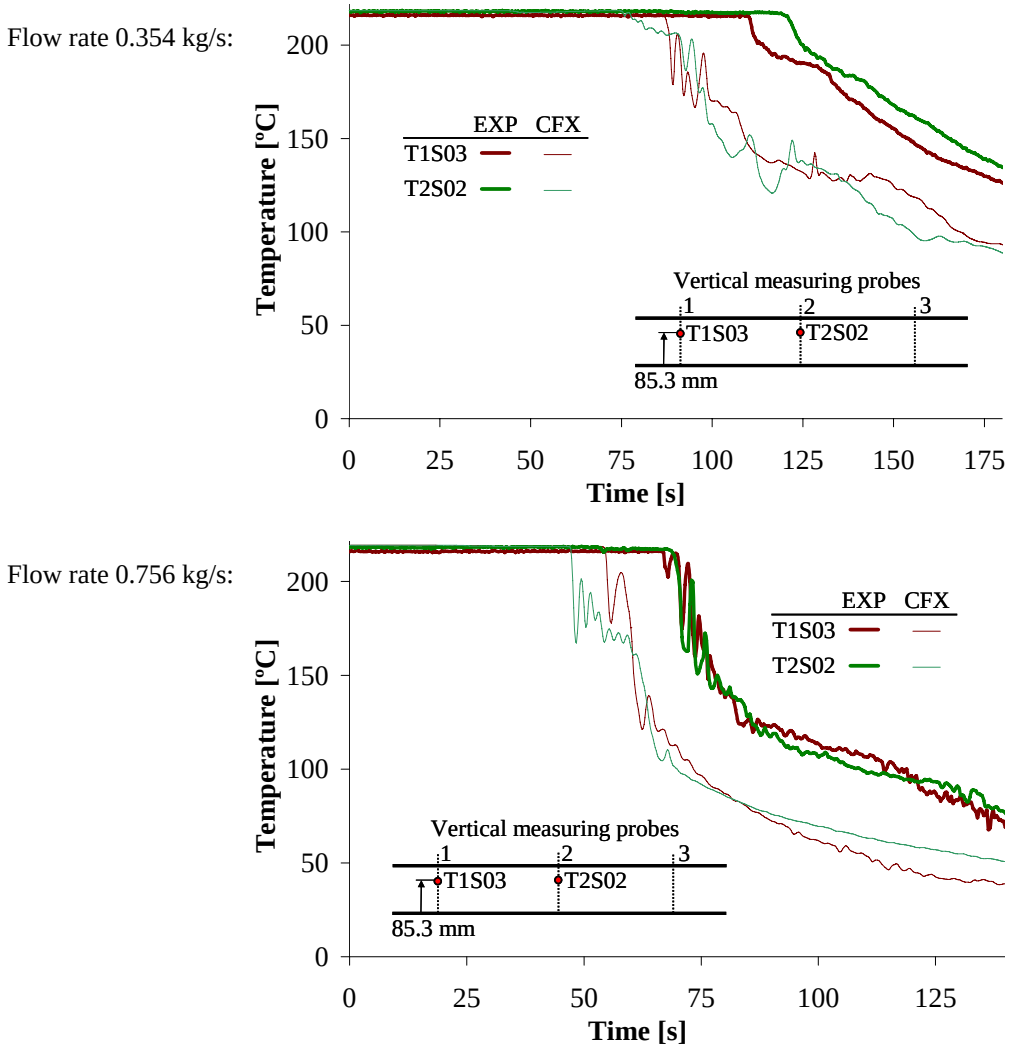

Figure 8. Temperature evolutions along the higher region of the horizontal pipe for two flow rates.

Figure 9 shows the temperature distributions along the vertical diameter of the measuring station 1. Data were taken at 80 s for the flow rate 0.354 kg/s, 50 s for the flow rate 0.756 kg/s and 40 s for the flow rate 1.06 kg/s. The high temperature gradients characterize thermal stratification occurrence for all the flow rates.

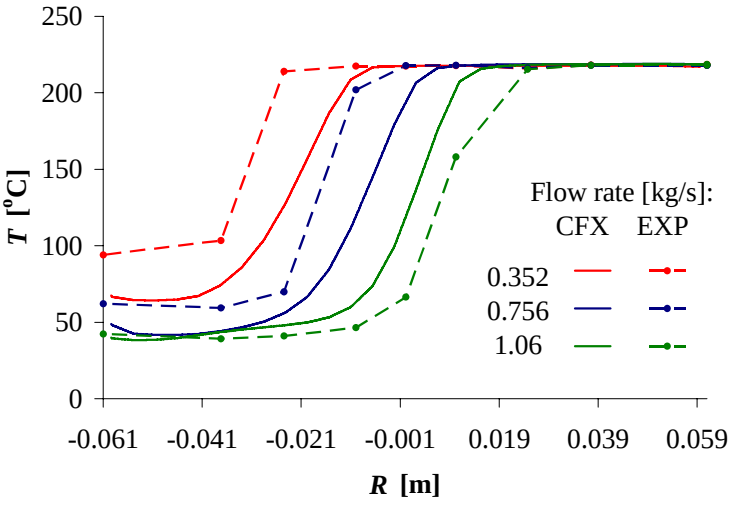

Figure 9. Temperature distributions along the vertical diameter of measuring station 1.

Figures 10 show the temperature evolution at three thermocouples positioned at the middle height of the measuring station 2 for the experiments at flow rate 0.756 kg/s. Thermocouple T2S04 was positioned in the center of the tube at the vertical probe, thermocouple T2I15 was positioned 3 mm away from the inside wall and thermocouple T2E11 was brazed on the outside wall.

Both numerical and experimental simulations show small temperature differences between thermocouple positions T2S04 and T2I15 but differences superior to 50 °C between these temperatures and the tubes external surface temperatures (T2E11).

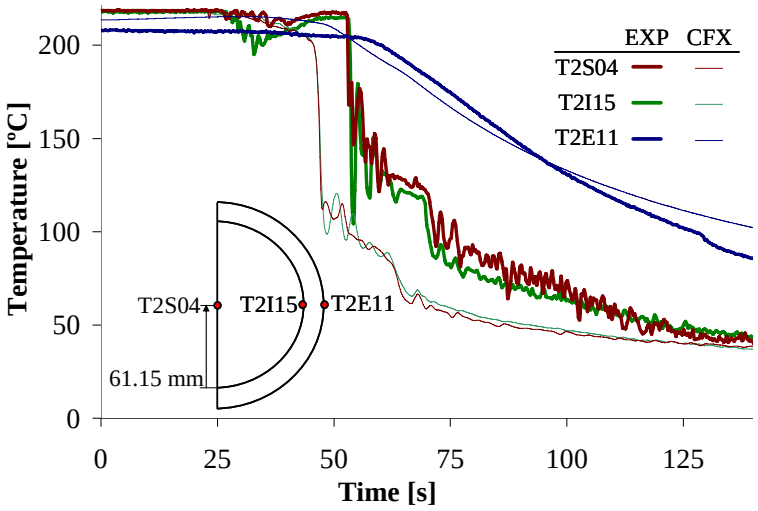

Figure 10. Temperature evolution at the middle high at measuring station 2 for flow rate 0.756 kg/s.

Figure 11 shows the evolution of the temperature difference, Eq. (2), between the average temperature on the highest position of the horizontal tube and the average temperature on the lowest position of the same tube. These averages were obtained from the positions of the highest wall thermocouples at measuring stations 1 and 2 and from the lowest positions of the wall thermocouples at the same measuring stations. The temperature differences, *DT*, for the highest and lowest inside thermocouples, 3 mm from the wall, are also shown in Fig. 11.

$$DT = \left[\left(T_1^u + T_2^u\right) - \left(T_1^l + T_2^l\right)\right] / 2 \tag{2}$$

where the superscripts u and l are relative to the upper and the lower positions and subscripts 1 and 2 to the first and the second measuring station of the horizontal tube.

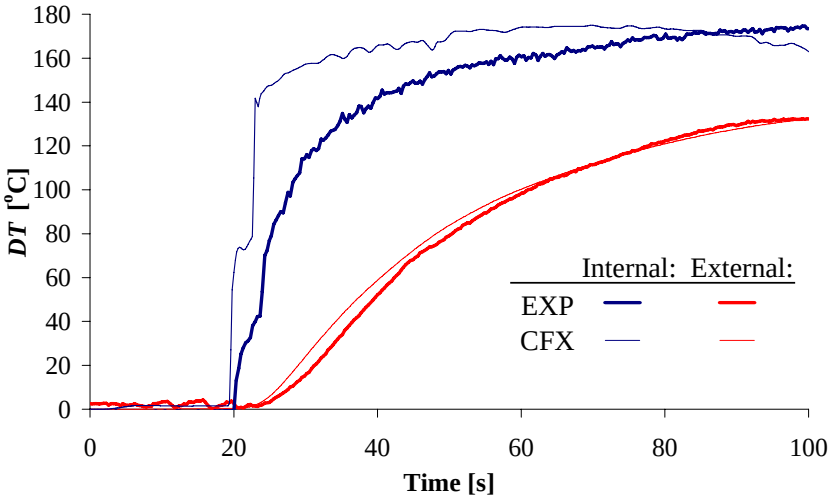

Figure 11. Temperature difference between the upper and the lower part of the horizontal pipe for flow rate 0.756 kg/s.

Figure 11 shows temperature differences up to 180 °C between the upper and lower internal averages and up to 120 °C between the upper and lower external averages.

5. CONCLUSIONS

The one phase thermal stratification was simulated numerically and experimentally in a piping system similar to the steam generator injection nozzle at the secondary loop of a Pressurized Water Reactor (PWR). The simulations were carried out with Froude numbers close to nuclear reactors operation ($Fr \cong 0.063$, 0.146 and 0.205) and a great temperature gradient was obtained, characterizing thermal stratification.

Despite the simplifications assumed in the numerical simulations its results presented a satisfactory agreement with the experimental results in the lower region of the horizontal pipe. In the upper region, the temperature drops due to the cold water front arrival calculated by the CFX 10.0 occur earlier than those obtained experimentally. The experimental thermocouple distribution together with the data collecting frequency was enough to detect the oscillation of the interface between cold and hot water layers (striping). These oscillations were also obtained in the numerical simulation. Numerical simulations using better mesh and time step refinement with a LES (Large Eddy Simulation) methodology and other RANS turbulence models should be appraised. In spite of the differences between the experimental and numerical results, the numerical methodology can be considered a good additional tool for predicting thermal stratification behavior and planning experiments.

6. REFERENCES

CFX-10.0, 2005, “User manual”, ANSYS-CFX.

Häfner, W., 1990, “Thermische Schichit-Versuche im horizontalen Rohr”, Kernforschungszentrum Karlsruhe GmbH, Karlsruhe, Germany , 238 p.

Poussin, C. and Holcblat, A., 1995, “Framatome antistratification device for steam generator feedwater nozzle: effectiveness, qualification test, and on-site measurements”, Nuclear Technology, Vol. 112, pp. 108 – 121.

Schuler, X. and Herter, K. H., 2004, “Thermal fatigue due to stratification and thermal shock loading of piping”, 30th MPA – Seminar in conjunction with the 9th German-Japanese Seminar, Stuttgart, Germany, pp. 6.1 – 6.14.

Ware, A. G..; Shah, V. N., 1995, “Fatigue monitoring in nuclear power plants.” Water Reactor Safety Information Meeting, Washington, DC, Vol. 3, pp. 227 – 249.

7. RESPONSIBILITY NOTICE

The authors are the only responsible for the printed material included in this paper.